TR－H－037

Multi-Valued Standard Regularization Theory (1): Global Reconstruction of Multiple Transparent Surfaces via Massively Parallel Relaxation Algorithms

Masahiko SHIZAWA

1993. 10. 25

ATR人間情報通信研究所

〒619-02 京都府相楽郡精華町光台2-2　☎07749-5-1011

ATR Human Information Processing Research Laboratories

2-2, Hikaridai, Seika-cho, Soraku-gun, Kyoto 619-02 Japan

Telephone: +81-7749-5-1011
Facsimile: +81-7749-5-1008

Multi-Valued Standard Regularization Theory (1): Global Reconstruction of Multiple Transparent Surfaces via Massively Parallel Relaxation Algorithms [1]

Masahiko Shizawa
ATR Human Information Processing Research Laboratories

[1]This paper is submitted to the Third European Conference on Computer Vision (ECCV'94)

Abstract

A fundamental extension of the standard regularization theory is proposed for data approximations by multi-valued functions which are essential for such as the transparency problems in computational vision. Conventional standard regularization theory can approximate scattered data by a single-valued function which is smooth everywhere in the domain. However, to incorporate discontinuities of the functions, we need to introduce the line process or equivalent techniques for breaking the coherence or smoothness of the approximating functions. Multi-layer representations have recently been used for multiple overlapping surface reconstruction. However, this should incorporate auxiliary fields for segmenting the given data. Further, these two different approaches share the difficulty of implementing optimizations of their energy functionals, since they become non-quadratic, non-convex minimization problems with respect to unknown surface and auxiliary field parameters. In this paper, by using a direct representation for multi-fold surfaces, we show that the data approximation by a multi-valued function can be reduced to minimization of a single quadratic convex functional. Therefore, since the Euler-Lagrange equation of the functional becomes linear, we can get benefit from simple relaxation techniques of guaranteed convergence to the optimal solution.

Keywords

Standard regularization theory, Surface reconstruction, Multi-valued functions, Transparency, Optimization.

Acknowledgments

The author thanks Prof. Tomaso Poggio and Dr. Federico Girosi of MIT Artificial Intelligence Laboratories for discussions and helpful comments during their visit to ATR. He also thanks Drs. Masa'aki Sato and Hiroshi Ando, Mr. Hideki Hayakawa and Mr. Hiroyuki Mizutani for their comments on the early Japanese draft version of this paper. Further, the author thanks Mr. Tadashi Takumi of CSK Corporation for algorithm implementations on CM-2. Finally, he thanks Dr. Yoh'ichi Tohkura, president of ATR Human Information Processing Research Laboratories and Dr. Shigeru Akamatsu, head of department #3 for their support.

Contents

1 Introduction

The regularization theory is a general framework for solving ill-posed inverse problems in computational vision [17] [18] [27]. Surface reconstruction from sparse data, edge detection, optical flow, and shape from shading, etc. have been formulated using the regularization principle[17]. Regularization theory also provides a universal and very useful mathematical framework for solving inverse problems in various engineering numerical analyses as well as in biological information sciences[20]. However, the *standard* regularization theory can only serve for recovering *continuous, single-valued* functions. Therefore, it cannot handle discontinuities of the functions and multi-valuedness of surfaces that are required to reconstruct multiple overlapping surfaces.

To incorporate surface discontinuities, Geman & Geman introduced the *line process* which inhibits propagation of smoothness across the discontinuities. Terzopoulos has proposed adaptive control of the regularization parameters so that the smoothness constraint vanishes at the surface discontinuities. Various improvements and approximations for thsese approaches have been suggested, for example Refs.[2][5].

The control of the smoothness terms using such a line process alone cannot handle transparency in which the sample data is a complete mixture of data on multiple surfaces, since it produces a solution of discontinuities almost everywhere on the surface in extreme cases. *Multi-layer representations* have recently been suggested for these cases. For example, Darrel et. al.[3] proposed an optimization framework for segmenting and decomposing an intensity image into a multi-layer representation. Darrel & Pentland used their framework to the segmentation of motion images[4]. Wang & Adelson[28] and Madarasmi[12] applied the multi-layer representation to motion analysis and stereo transparency, respectively. However, these approaches cannot handle the cases where multiple values are assigned to a single point, in other words, the case of *multi-valued data.* Ando [1] developed an optimization framework for surface reconstruction using the multi-layer representation in which each data point has a variable indicating the surface to which the data point assigned. It is therefore capable of handling multi-valued data. Another possible solution to the transparency problem is to represent multiple attributes as a multi-modal distribution [13] [14] [15].

The above approaches used auxiliary or extremely redundant parameters such as line process field, data assignment variables for clustering, and the

distribution fields. Therefore, they cannot be simple and reliable in their optimizations since the problems become minimizations of non-quadratic, non-convex energy functionals. For example, Darrel & Pentland used the Simulated Annealing method, and Madarasmi and Ando used the Mean Field Annealing method to minimize their energy functionals.

This paper provides a general computational framework for representing multi-valued functions in a single equation without introducing any auxiliary parameters other than component functions. Based on this representation, we formulate the reconstruction problem of multiple overlapping surfaces as a *standard regularization problem.* Since the energy functional becomes quadratic and convex, its Euler-Lagrange equation turns out to be linear. Therefore, we can use optimization techniques that can be implemented by using simple relaxation, for example, the steepest descent and Gauss-Seidel methods. These optimization methods guarantee convergence to the optimal solution under general conditions. Therefore, our framework has a great advantage over conventional multi-layer representations and their optimization algorithms. We call this extension of the standard regularization theory *Multi-Valued Standard Regularization Theory* which we abbreviate to MVSRT in this paper.

The paper is organized as follows.

In Sec. 2, we demonstrate the capabilities of MVSRT by deriving a two-fold surface reconstruction algorithm based on discrete approximation and the Gauss-Seidel relaxation method. Several simulations under various conditions are performed on the algorithm.

Sec. 3 provides the general theory of MVSRT for h-valued scalar functions. Further, extensions to multi- and vector-valued function are also discussed by using the tensor product.

Sec. 4 concludes this paper and discusses remaining problems.

2 Multiple-Surface Reconstruction via Standard Regularization Theory

In this section, we derive a regularization algorithm for solving two-fold-surface reconstruction problems. The transparency problems in computational vision generally require recovery of multiple overlapping surfaces from possibly multi-valued data (see Fig. 1 and Ref. [24]). In the case of transparency, surfaces must be recovered even if the data is partially lacking such as for the upper surface in Fig. 1. Therefore, the surface recovery algorithm must be global optimization rather than local optimization. The regularization theory helps to solve this problem if it is extended to the multi-valued functional approximation.

2.1 Energy Functional for Two-fold-surface Reconstruction

The conventional standard regularization problem for single-valued functional approximation is formulated as a minimization of the following quadratic energy functional [17].

$$E^{(1)}[f] = \sum_{i=1}^{N} \left(y_{(i)} - f(\mathbf{x}_{(i)})\right)^2 + \lambda \|Sf(\mathbf{x})\|^2 \qquad (1)$$

where, S is the regularization (smoothness) operator, λ is the regularization weight parameter, and $\|\ \ \|$ is the norm of the functional space. $(\mathbf{x}_{(i)}, y_{(i)})$ denotes the i-th data where $i = 1, 2, \cdots, N$.

In this case, we can see that the constraint for the data is $y = f(\mathbf{x})$. If we define two overlapping surfaces by $y = f_1(\mathbf{x})$ and $y = f_2(\mathbf{x})$, we can write the constraint of the two-fold surface in a single equation,

$$(y - f_1(\mathbf{x}))\,(y - f_2(\mathbf{x})) = y^2 - (f_1(\mathbf{x}) + f_2(\mathbf{x}))\,y + f_1(\mathbf{x}) f_2(\mathbf{x}) = 0. \qquad (2)$$

Figure 2 shows the two-fold surface defined by this equation. This is the necessary and sufficient condition for each data point being placed on either of two surfaces. Since real data has noise, we can consider that each data point is approximated by either of two surfaces. An advantage of this representation is that two surfaces can be represented in a single equation without explicitly

indicating the assignment of the data points. Therefore, it is not necessary to introduce an auxiliary field such as an integer variable indicating assignment of data points.

Next, we define functions $F(\mathbf{x})$ and $G(\mathbf{x})$ as follows.

$$\begin{aligned} F(\mathbf{x}) &= f_1(\mathbf{x}) f_2(\mathbf{x}), \\ G(\mathbf{x}) &= -\left(f_1(\mathbf{x}) + f_2(\mathbf{x})\right) \end{aligned} \tag{3}$$

Therefore, Eq. (2) becomes linear with respect to unknown functions $F(\mathbf{x})$ and $G(\mathbf{x})$ as

$$F(\mathbf{x}) + G(\mathbf{x}) y + y^2 = 0. \tag{4}$$

The inverse transformation of (3) can be written as

$$f_1(\mathbf{x}), f_2(\mathbf{x}) = \frac{1}{2}\left[-G(\mathbf{x}) \pm \sqrt{\{G(\mathbf{x})\}^2 - 4F(\mathbf{x})}\right]. \tag{5}$$

Both the transformation (3) and the inverse transformation (5) are smooth, differentiable and nonsingular except when $f_1(\mathbf{x}) = f_2(\mathbf{x})$, i.e., when the surfaces intersect each other and when the surfaces degenerate into a single surface. If we adopt the smoothness constraint on the original functions, we have nonlinear Euler-Lagrange equations that are difficult to solve in a simple scheme. Thus, instead of imposing the smoothness constraint on the original functions $f_1(\mathbf{x})$ and $f_2(\mathbf{x})$, it is a reasonable compromise to use the smoothness constraint on the transformed functions $F(\mathbf{x})$ and $G(\mathbf{x})$. Thus, we have a quadratic convex energy functional in both the data term and the regularization terms. In other words, the problem can be transformed into the *standard regularization problem.*

It should be noted, however, that the inverse transformation (5) has an inevitable ambiguity in determining correspondence to the original functions $f_1(\mathbf{x})$ and $f_2(\mathbf{x})$. This is due to the fact that the constraint equation (2) and the transformation (3) have a symmetry of permutation between the functions $f_1(\mathbf{x})$ and $f_2(\mathbf{x})$. In fact, we cannot determine which of two functions on the right hand side of Eq. (5) corresponds to $f_1(\mathbf{x})$ (and to $f_2(\mathbf{x})$). A problem emerges if the surfaces intersect since, at the point of intersection, we have indeterminacy in connection of surfaces. However, this situation is rare in nature and to the author's knowledge there is no psychophysical evidence that humans have the capability of perceiving intersecting surfaces (for example, in binocular stereo vision).

Now we have a quadratic energy functional for the standard regularization problem of a two-fold surface as follows.

$$E^{(2)}[F,G] = \sum_{i=1}^{N}\left\{F(\mathbf{x}_{(i)}) + G(\mathbf{x}_{(i)})y_{(i)} + \left(y_{(i)}\right)^2\right\}^2 + \lambda_F\|S_F F(\mathbf{x})\|^2 + \lambda_G\|S_G G(\mathbf{x})\|^2 \quad (6)$$

In this formalism, functions $F(\mathbf{x})$ and $G(\mathbf{x})$ may have arbitrary values, although the inverse transformation (5) requires the condition of real numbers for the square root.

$$\{G(\mathbf{x})\}^2 - 4F(\mathbf{x}) \geq 0 \quad (7)$$

Therefore, strictly speaking, the problem must be formulated as a constrained optimizations with this inequality. However, we have not yet detected this case in our simulations even in the transient conditions. In practice, it may not be necessary to implement this constraint in optimizations of Eq. (6). We may be able to detect this improper unreliable case by testing Eq.(7) after the optimization. This fact may simplify analog hardware implementations. In fact, the optimization problem of the energy functional (6) is similar to the regularization of optical flow fields[9].

2.2 Gauss-Seidel Relaxation Algorithm for Optimization

In this subsection, we derive an optimization algorithm for MVSRT using Gauss-Seidel relaxation by a discrete approximation which is a popular massively-parallel implementation for the standard regularization theory. We use the membrane model for the regularization operator $S_F = S_G = \nabla = \left(\frac{\partial}{\partial x_1}, \frac{\partial}{\partial x_2}\right)$. In the following, we assume that the variables x_1 and x_2 take integer values. Therefore, the energy functional (6) is approximated by

$$\begin{aligned}\mathcal{E}^{(2)}(F,G) = &\sum_{i=1}^{N}\left\{F_{x_{1(i)},x_{2(i)}} + G_{x_{1(i)},x_{2(i)}}y_{(i)} + \left(y_{(i)}\right)^2\right\}^2 \\ &+ \sum_{(x_1,x_2)\in Z^2}\lambda_F\{(F_{x_1,x_2} - F_{x_1-1,x_2})^2 + (F_{x_1,x_2} - F_{x_1,x_2-1})^2\} \\ &+ \sum_{(x_1,x_2)\in Z^2}\lambda_G\{(G_{x_1,x_2} - G_{x_1-1,x_2})^2 + (G_{x_1,x_2} - G_{x_1,x_2-1})^2\} \quad (8)\end{aligned}$$

where F_{x_1,x_2} and G_{x_1,x_2} are values of $F(\mathbf{x})$ and $G(\mathbf{x})$ at grid points $(x_1, x_2) \in \boldsymbol{Z}^2$. $\left\{(x_{1(i)}, x_{2(i)}), y_{(i)}\right\}$ $(i = 1, \cdots, N)$ are sparse sample data points and values given at the points.

To minimize the energy functional (8), we derived the following Euler-Lagrange equation by taking the partial derivatives with respect to F_{x_1,x_2} and G_{x_1,x_2} and equating them to zeros.

$$\begin{aligned}
\frac{\partial \mathcal{E}^{(2)}(F,G)}{\partial F_{x_1,x_2}} &= 2\left[\sum_{i=1}^{N} \delta_{x_1,x_{1(i)}}\delta_{x_2,x_{2(i)}}\left\{F_{x_{1(i)},x_{2(i)}} + G_{x_{1(i)},x_{2(i)}}y_{(i)} + \left(y_{(i)}\right)^2\right\}\right] \\
&\quad +2\lambda_F\left(F_{x_1,x_2} - \bar{F}_{x_1,x_2}\right) = 0, \\
\frac{\partial \mathcal{E}^{(2)}(F,G)}{\partial G_{x_1,x_2}} &= 2\left[\sum_{i=1}^{N} \delta_{x_1,x_{1(i)}}\delta_{x_2,x_{2(i)}}\left\{F_{x_{1(i)},x_{2(i)}}y_{(i)} + G_{x_{1(i)},x_{2(i)}}\left(y_{(i)}\right)^2 + \left(y_{(i)}\right)^3\right\}\right] \\
&\quad +2\lambda_G\left(G_{x_1,x_2} - \bar{G}_{x_1,x_2}\right) = 0,
\end{aligned} \tag{9}$$

where $\delta_{a,b}$ is Kronecker's delta, i.e., when $a = b$, it equals 1 and otherwise equals 0. $\bar{F}_{x_1,x_2}$ and $\bar{G}_{x_1,x_2}$ are averages of four neighborhoods F_{x_1-1,x_2}, F_{x_1+1,x_2}, F_{x_1,x_2-1}, F_{x_1,x_2+1} and G_{x_1-1,x_2}, G_{x_1+1,x_2}, G_{x_1,x_2-1}, G_{x_1,x_2+1}, respectively,

$$\begin{aligned}
\bar{F}_{x_1,x_2} &= \frac{1}{4}\left(F_{x_1+1,x_2} + F_{x_1-1,x_2} + F_{x_1,x_2+1} + F_{x_1,x_2-1}\right), \\
\bar{G}_{x_1,x_2} &= \frac{1}{4}\left(G_{x_1+1,x_2} + G_{x_1-1,x_2} + G_{x_1,x_2+1} + G_{x_1,x_2-1}\right)
\end{aligned} \tag{10}$$

Next, we define the following quantities just like moments which can be computed directly from the sample data.

$$\begin{aligned}
A_{x_1,x_2} &= \sum_{i=1}^{N} \delta_{x_1,x_{1(i)}}\delta_{x_2,x_{2(i)}}, \\
B_{x_1,x_2} &= \sum_{i=1}^{N} \delta_{x_1,x_{1(i)}}\delta_{x_2,x_{2(i)}}y_{(i)}, \\
C_{x_1,x_2} &= \sum_{i=1}^{N} \delta_{x_1,x_{1(i)}}\delta_{x_2,x_{2(i)}}\left(y_{(i)}\right)^2, \\
D_{x_1,x_2} &= \sum_{i=1}^{N} \delta_{x_1,x_{1(i)}}\delta_{x_2,x_{2(i)}}\left(y_{(i)}\right)^3
\end{aligned} \tag{11}$$

These quantities are all zero for points where there is no data. It is important to note that this formalism can admit *multi-valued data*, and also *multiple data* may be overlapping at the same point. There is no restriction on the multi-valuedness at each point. This is significant especially for the case of 'pure' transparency, where multiple attributes are truly overlapped.

Using the above notations, we have the following simplified version of the Euler-Lagrange equation.

$$\begin{aligned} (A_{x_1,x_2} + \lambda_F) F_{x_1,x_2} + B_{x_1,x_2} G_{x_1,x_2} &= \lambda_F \bar{F}_{x_1,x_2} - C_{x_1,x_2}, \\ B_{x_1,x_2} F_{x_1,x_2} + (C_{x_1,x_2} + \lambda_G) G_{x_1,x_2} &= \lambda_G \bar{G}_{x_1,x_2} - D_{x_1,x_2}. \end{aligned} \tag{12}$$

By solving these simultaneous linear equations with respect to F_{x_1,x_2} and G_{x_1,x_2}, we have the following equations.

$$\begin{aligned} F_{x_1,x_2} &= \frac{\lambda_F (C_{x_1,x_2} + \lambda_G) \bar{F}_{x_1,x_2} - \lambda_G B_{x_1,x_2} \bar{G}_{x_1,x_2} + B_{x_1,x_2} D_{x_1,x_2} - C_{x_1,x_2} (C_{x_1,x_2} + \lambda_G)}{(A_{x_1,x_2} + \lambda_F)(C_{x_1,x_2} + \lambda_G) - B^2_{x_1,x_2}}, \\ G_{x_1,x_2} &= \frac{-\lambda_F B_{x_1,x_2} \bar{F}_{x_1,x_2} + \lambda_G (A_{x_1,x_2} + \lambda_F) \bar{G}_{x_1,x_2} + B_{x_1,x_2} C_{x_1,x_2} - D_{x_1,x_2} (A_{x_1,x_2} + \lambda_F)}{(A_{x_1,x_2} + \lambda_F)(C_{x_1,x_2} + \lambda_G) - B^2_{x_1,x_2}} \end{aligned} \tag{13}$$

Thus, we have the following massively parallel Gauss-Seidel relaxation algorithm.

$$\begin{aligned} F^{[k+1]}_{x_1,x_2} &= a_{x_1,x_2} \bar{F}^{[k]}_{x_1,x_2} + b_{x_1,x_2} \bar{G}^{[k]}_{x_1,x_2} + p_{x_1,x_2}, \\ G^{[k+1]}_{x_1,x_2} &= c_{x_1,x_2} \bar{F}^{[k]}_{x_1,x_2} + d_{x_1,x_2} \bar{G}^{[k]}_{x_1,x_2} + q_{x_1,x_2} \end{aligned} \tag{14}$$

where k is an index of iterative operations, and a_{x_1,x_2}, $b_{x_1.x_2}$, c_{x_1,x_2}, d_{x_1,x_2}, p_{x_1,x_2}, and q_{x_1,x_2} are quantities which are computed at each lattice point prior to the relaxation. They are defined as

$$\begin{aligned} a_{x_1,x_2} &= \lambda_F (C_{x_1,x_2} + \lambda_G) / U_{x_1,x_2}, \\ b_{x_1,x_2} &= -\lambda_G B_{x_1,x_2} / U_{x_1,x_2}, \\ c_{x_1,x_2} &= -\lambda_F B_{x_1,x_2} / U_{x_1,x_2}, \\ d_{x_1,x_2} &= \lambda_G (A_{x_1,x_2} + \lambda_F) / U_{x_1,x_2}, \\ p_{x_1,x_2} &= \{B_{x_1,x_2} D_{x_1,x_2} - C_{x_1,x_2} (C_{x_1,x_2} + \lambda_G)\} / U_{x_1,x_2}, \\ q_{x_1,x_2} &= \{B_{x_1,x_2} C_{x_1,x_2} - D_{x_1,x_2} (A_{x_1,x_2} + \lambda_F)\} / U_{x_1,x_2} \end{aligned} \tag{15}$$

where $U_{x_1,x_2} = (A_{x_1,x_2} + \lambda_F)(C_{x_1,x_2} + \lambda_G) - B^2_{x_1,x_2}$. Note that at points having no data, $a_{x_1,x_2} = d_{x_1,x_2} = 1, b_{x_1,x_2} = c_{x_1,x_2} = p_{x_1,x_2} = q_{x_1,x_2} = 0$ and therefore, the relaxation becomes a filling-in process.

This algorithm can be implemented by the massively-parallel network shown in Fig. 4.

2.3 Steepest Descent Algorithm for Optimization

Another algorithm is possible for minimization of the function (9). The equilibrium point of the following linear dynamical system provides the optimal solution. This formalism is important for analog hardware implementation.

$$\frac{dF(\mathbf{x})}{dt} = -\omega \frac{\delta E^{(2)}[F,G]}{\delta F(\mathbf{x})}, \quad \frac{dG(\mathbf{x})}{dt} = -\omega \frac{\delta E^{(2)}[F,G]}{\delta G(\mathbf{x})}. \tag{16}$$

Discrete approximation of this scheme is the steepest descent algorithm.

$$\begin{aligned} F^{[k+1]}_{x_1,x_2} &= F^{[k]}_{x_1,x_2} - 2\omega\{(A_{x_1,x_2} + \lambda_F) F^{[k]}_{x_1,x_2} \\ &+ B_{x_1,x_2} G^{[k]}_{x_1,x_2} + C_{x_1,x_2} - \lambda_F \bar{F}^{[k]}_{x_1,x_2}\}, \\ G^{[k+1]}_{x_1,x_2} &= G^{[k]}_{x_1,x_2} - 2\omega\{B_{x_1,x_2} F^{[k]}_{x_1,x_2} \\ &+ (C_{x_1,x_2} + \lambda_G) G^{[k]}_{x_1,x_2} - D_{x_1,x_2} - \lambda_G \bar{G}^{[k]}_{x_1,x_2}\} \end{aligned} \tag{17}$$

This technique is not suitable for digital computers, since its convergence is very slow.

2.4 Simulation Results

We performed computer simulations by using data sets for various conditions. We show several results from these simulations in this subsection.

We discretized the space of $\mathbf{x}$ into 512×512 in a 2-dimensional array. The optimization algorithm is based essentially on the Gauss-Seidel relaxation which was derived in section 2.2. The algorithm was implemented on a CM-2 massively parallel processor.

Figure 5 shows the results of the first experiment for two planar surfaces $y = f_1(\mathbf{x}) = 0.8$ and $y = f_2(\mathbf{x}) = -0.8$. 10000 points were randomly generated for each surface. Then, about 4000 points were removed from the upper surface so that the upper surface had striped areas with no supporting data. It should be noted that some data overlapped each other, i.e., they

were truly transparent, since we were not concerned about the generation of multiple points at the same position $\mathbf{x}$. We added Gaussian noise with standard deviation $\sigma = 0.05$. The regularization parameters were set at $\lambda_F = \lambda_G = 6.0$. As the results show, we have overlapping surfaces even in the area with no data on the upper surface. Human perception of this kind of 'ghost' surfaces, which can be seen as subjective transparency, is a familiar phenomenon [29] [10].

The second experiment (Fig. 6) demonstrates the capabilities for a 'discontinuous' surface. The data of the two surfaces are generated so that they form stripe patterns of reverse phase. The number of points on each surface were approximately 5000, and the other parameters were chosen in the same as in the first experiment.

The third, fourth and fifth experiments (Figs. 7, 8, 9) investigated the behavior when the algorithm was applied to complex situations. We used superposition of a planar surface and a surface with sine shape. Equations of these surfaces were

$$\begin{aligned} f_1(\mathbf{x}): &\quad -0.5 + N(0, \sigma^2), \\ f_2(\mathbf{x}): &\quad 2\sin 3\pi \left(\frac{x_2 - 256}{512}\right) + N(0, \sigma^2). \end{aligned} \tag{18}$$

$N(m, \sigma^2)$ denotes Gaussian noise of mean m and standard deviation σ. The number of data points and standard deviations of noise were as follows.

- Experiment #3: $N_1 = 10000$, $N_2 = 20000$, $\sigma = 0.05$
- Experiment #4: $N_1 = 10000$, $N_2 = 10000$, $\sigma = 2.0$
- Experiment #5: $N_1 = 1000$、 $N_2 = 10000$、 $\sigma = 0.05$

The regularization parameters were set at $\lambda_F = \lambda_G = 12.0$.

The initial values for the functions F and G in all the experiments were set to zero, i.e., $F^{[0]}_{x_1,x_2} = G^{[0]}_{x_1,x_2} = 0$.

2.4.1 Discussion

From the above simulations, we observe the following about the properties and problems of the theory and algorithm presented here.

1. From experiments #1 and #2, we see the capability of reconstructing transparent surfaces even if the data for the surfaces are partially lacking.

2. Experiment #2 is nothing but an active demonstration of Prazdny's idea of representing discontinuities by multiple overlapping surfaces [22].

3. Experiments #3-#5 show the capability and limitation of MVSRT for reconstructing nonplanar curved surfaces and intersections. The algorithm cannot directly represent intersection of surfaces. However, this limitation is common for other multi-layer representations. Although the reconstructed surfaces do not touch each other at the intersection point, we can detect the possible intersection by testing condition $\{G(\mathbf{x})\}^2 - 4F(\mathbf{x}) = 0$ of Eq. (7) using a certain threshold to account for the noise in the estimated functions.

4. From experiment #4, we see noise tolerance of MVSRT.

5. From experiment #5, we see that even if the density of sample data is not evenly distributed for the two surfaces (in this experiment, the ratio of the density is 10.0), the multiple-surface reconstruction succeeds.

In summary, MVSRT was verified for various conditions of noisy data.

3 General Theory of Multi-Valued Standard Regularization Theory

This section gives a general formulation and derives properties for MVSRT. First, we derive a constraint equation for the h-valued scalar function and standard regularization theory is applied to these constraints. Next, the theory is extended into vector-valued functions.

3.1 Regularization of h-valued scalar function

We assume that the data is to be modeled by overlapping h surfaces $y = f_i(\mathbf{x})$ $(i = 1, 2, \cdots, h)$. The constraint equation for the h-fold surface is:

$$\begin{aligned} &\prod_{i=1}^{h} (y - f_i(\mathbf{x})) = y^h - \pi_1^{(h)}(\mathbf{x}) y^{h-1} + \pi_2^{(h)}(\mathbf{x}) y^{h-2} - \cdots \\ &+(-1)^h \pi_h^{(h)}(\mathbf{x}) = 0 \end{aligned} \tag{19}$$

where $\pi_k^{(h)}(\mathbf{x})(k = 1, \cdots, h)$ are elementary symmetric expressions of $f_i(\mathbf{x})(i = 1, \cdots, h)$ defined by

$$\begin{aligned} \pi_1^{(h)}(\mathbf{x}) &= \sum_{i=1}^{h} f_i(\mathbf{x}), \\ \pi_2^{(h)}(\mathbf{x}) &= \sum_{i_1=1}^{h} \sum_{i_2=i_1+1}^{h} f_{i_1}(\mathbf{x}) f_{i_2}(\mathbf{x}), \\ &\cdots, \\ \pi_h^{(h)}(\mathbf{x}) &= f_1(\mathbf{x}) f_2(\mathbf{x}) \cdots f_h(\mathbf{x}). \end{aligned} \tag{20}$$

Then, we can formulate a regularization problem with respect to $\pi_k^{(h)}(\mathbf{x})$ instead of $f_i(\mathbf{x})$. The transformation (20) becomes singular mapping only when the h-degree algebraic equation with respect to y (19) has at least one multiple-root solution. Therefore, an inverse transformation exists except for this case.

The inverse transformation can be obtained by solving the h-degree algebraic equation with respect to ϕ:

$$\Lambda^{(h)}(\phi) = \phi^h - \pi_1^{(h)}(\mathbf{x}) \phi^{h-1} + \pi_2^{(h)}(\mathbf{x}) \phi^{h-2} - \cdots$$

$$+(-1)^h \pi_h^{(h)}(\mathbf{x}) = 0. \tag{21}$$

In a similar way to the case of a two-fold surface, an indeterminacy exists in the permutation between $f_i(\mathbf{x})(i = 1, 2, \cdots, h)$.

Therefore, the energy functional for the h-fold surface can generally be written as

$$\begin{aligned} &E^{(h)}[\pi_1^{(h)}, \pi_2^{(h)}, \cdots, \pi_h^{(h)}] = \\ &\sum_{i=1}^{N} \{y_{(i)}^h - \pi_1^{(h)}(\mathbf{x}_{(i)}) y_{(i)}^{h-1} + \pi_2^{(h)}(\mathbf{x}_{(i)}) y_{(i)}^{h-2} - \cdots \\ &+(-1)^h \pi_h^{(h)}(\mathbf{x}_{(i)})\}^2 + \sum_{k=1}^{h} \lambda_k \| S_k^{(h)} \pi_k^{(h)}(\mathbf{x}) \|^2. \end{aligned} \tag{22}$$

This energy functional is quadratic with respect to unknown functions $\pi_k^{(h)}(\mathbf{x})$. Therefore, its Euler-Lagrange equation becomes linear. This fact enables us to derive relaxation algorithms with guaranteed convergence to the optimal solution.

The solutions of the algebraic equation (21) can be implemented by several numerical methods for solving higher-order univariate algebraic equations. In our case, it is convenient for us if all the solutions are obtained simultaneously. The iterative method known as the Durand-Kerner method meets our purpose.

$$\phi_j^{[k+1]} = \phi_j^{[k]} - \frac{\Lambda^{(h)}(\phi_j^{[k]})}{\prod_{i=1, i \neq j}^{h} \left(\phi_j^{[k]} - \phi_i^{[k]}\right)}. \tag{23}$$

It is known that this is equivalent to the Newton-Raphson method applied to the simultaneous algebraic equation, Eq. (20). This algorithm does not work in the multiple root case. However, the exact multiple-root case does not occur in real cases of noisy data.

3.2 Extension to multi- and vector-valued functions

The regularization of vector-valued functions emerges when extracting optical flow[9]. One might think that the regularization of multi- and vector-valued functions can be simply achived by independently extending each

component of the vector into a multi-valued function. However, the multi-valuedness causes ambiguities in correspondence between components of the vector. Therefore, a more accurate model should be incorporated.

In the case of vector-valued functions, $\mathbf{y} = \mathbf{f}(\mathbf{x})$ ($\mathbf{y} \in R^m, \mathbf{x} \in R^n$), the constraint for MVSRT must be formulated by using the tensor product as follows. Suppose each function $\mathbf{f}_k(\mathbf{x})(k = 1, 2, \cdots, h)$ corresponds to each vector field. The direct constraint for the h-valued function is given by

$$(\mathbf{y} - \mathbf{f}_1(\mathbf{x})) \otimes (\mathbf{y} - \mathbf{f}_2(\mathbf{x})) \otimes \cdots \otimes (\mathbf{y} - \mathbf{f}_h(\mathbf{x})) = \mathbf{0}, \tag{24}$$

where $\otimes$ denotes the tensor product (Kronecker's product). This formalism has redundancy in the number of component equations. Actually, the number of component equations in Eq. (24) is m^h, although the number of original components is m. To reduce this redundancy, we can symmetrize the order of functions in Eq. (24). We then have ${}_mH_h$ component equations. There is still redundancy. However, this redundancy is only used for removing the ambiguity of the correspondences between components of the vector-values.

3.2.1 Constraints for the case of $h = 2$ and $n = 2$

In the following, to explain these issues, we show MVSRT of the case $h = 2$ and $m = 2$, i.e., the two-valued 2-dimensional vector-valued function in detail. In this case, the constraint can be written as

$$\frac{1}{2}\{(\mathbf{y} - \mathbf{f}_1(\mathbf{x})) \otimes (\mathbf{y} - \mathbf{f}_2(\mathbf{x})) + (\mathbf{y} - \mathbf{f}_2(\mathbf{x})) \otimes (\mathbf{y} - \mathbf{f}_1(\mathbf{x}))\} = \mathbf{0}, \tag{25}$$

where we denote the two two-dimensional vector-valued functions by

$$\begin{aligned} \mathbf{y} &= \mathbf{f}_1(\mathbf{x}) = (f_{1,1}(\mathbf{x}), f_{1,2}(\mathbf{x}))^T, \\ \mathbf{y} &= \mathbf{f}_2(\mathbf{x}) = (f_{2,1}(\mathbf{x}), f_{2,2}(\mathbf{x}))^T. \end{aligned} \tag{26}$$

Constraint (25) can be written in component form as

$$\begin{aligned} &y_1^2 - (f_{1,1}(\mathbf{x}) + f_{2,1}(\mathbf{x}))\, y_1 + f_{1,1}(\mathbf{x}) f_{2,1}(\mathbf{x}) = 0, \\ &y_2^2 - (f_{1,2}(\mathbf{x}) + f_{2,2}(\mathbf{x}))\, y_2 + f_{1,2}(\mathbf{x}) f_{2,2}(\mathbf{x}) = 0, \\ &2y_1 y_2 - (f_{1,2}(\mathbf{x}) + f_{2,2}(\mathbf{x}))\, y_1 - (f_{1,1}(\mathbf{x}) + f_{2,1}(\mathbf{x}))\, y_2 \\ &+ (f_{1,1}(\mathbf{x}) f_{2,2}(\mathbf{x}) + f_{1,2}(\mathbf{x}) f_{2,1}(\mathbf{x})) = 0. \end{aligned} \tag{27}$$

These constraints can be transformed into the following linear forms with respect to functions $F_1(\mathbf{x})$, $G_1(\mathbf{x})$, $F_2(\mathbf{x})$, $G_2(\mathbf{x})$ and $H(\mathbf{x})$.

$$\begin{aligned} &y_1^2 + G_1(\mathbf{x})y_1 + F_1(\mathbf{x}) = 0, \\ &y_2^2 + G_2(\mathbf{x})y_2 + F_2(\mathbf{x}) = 0, \\ &2y_1y_2 + G_2(\mathbf{x})y_1 + G_1(\mathbf{x})y_2 + H(\mathbf{x}) = 0. \end{aligned} \tag{28}$$

where

$$\begin{aligned} F_1(\mathbf{x}) &= f_{1,1}(\mathbf{x})f_{2,1}(\mathbf{x}), \\ F_2(\mathbf{x}) &= f_{1,2}(\mathbf{x})f_{2,2}(\mathbf{x}), \\ G_1(\mathbf{x}) &= -\left(f_{1,1}(\mathbf{x}) + f_{2,1}(\mathbf{x})\right), \\ G_2(\mathbf{x}) &= -\left(f_{1,2}(\mathbf{x}) + f_{2,2}(\mathbf{x})\right), \\ H(\mathbf{x}) &= f_{1,1}(\mathbf{x})f_{2,2}(\mathbf{x}) + f_{1,2}(\mathbf{x})f_{2,1}(\mathbf{x}). \end{aligned} \tag{29}$$

3.2.2 Regularization problem for $h = 2$ and $n = 2$ (1)

Constraints (28) can be used to determine unknown functions $F_1(\mathbf{x})$, $F_2(\mathbf{x})$, $G_1(\mathbf{x})$, $G_2(\mathbf{x})$, and $H(\mathbf{x})$ by the following *standard regularization problem.*

$$\begin{aligned} &E^{(2,2)}[F_1, F_2, G_1, G_2, H] = \\ &\sum_{i=1}^{N} \left\{ \left(y_{1(i)}\right)^2 + G_1(\mathbf{x}_{(i)})y_{1(i)} + F_1(\mathbf{x}_{(i)}) \right\}^2 \\ &+ \sum_{i=1}^{N} \left\{ \left(y_{2(i)}\right)^2 + G_2(\mathbf{x}_{(i)})y_{2(i)} + F_2(\mathbf{x}_{(i)}) \right\}^2 \\ &+ \frac{1}{2} \sum_{i=1}^{N} \left\{ 2y_{1(i)}y_{2(i)} + G_2(\mathbf{x}_{(i)})y_{1(i)} + G_1(\mathbf{x}_{(i)})y_{2(i)} + H(\mathbf{x}_{(i)}) \right\}^2 \\ &+ \lambda_{F_1} \|S_{F_1}F_1(\mathbf{x})\|^2 + \lambda_{F_2} \|S_{F_2}F_2(\mathbf{x})\|^2 \\ &+ \lambda_{G_1} \|S_{G_1}G_1(\mathbf{x})\|^2 + \lambda_{G_2} \|S_{G_2}G_2(\mathbf{x})\|^2 + \lambda_H \|S_H H(\mathbf{x})\|^2 \end{aligned} \tag{30}$$

where λ_{F_1}, λ_{F_2}, λ_{G_1}, λ_{G_2}, and λ_H are regularization parameters, and S_{F_1}, S_{F_2}, S_{G_1}, S_{G_2}, and S_H are regularization operators for functions $F_1(\mathbf{x})$, $F_2(\mathbf{x})$, $G_1(\mathbf{x})$, $G_2(\mathbf{x})$, and $H(\mathbf{x})$ respectively. In this case, the number of 'linear' functions $F_1(\mathbf{x})$, $F_2(\mathbf{x})$, $G_1(\mathbf{x})$, $G_2(\mathbf{x})$, and $H(\mathbf{x})$ are greater than the number of original functions $f_{1,1}(\mathbf{x})$, $f_{1,2}(\mathbf{x})$, $f_{2,1}(\mathbf{x})$ and $f_{2,2}(\mathbf{x})$. Therefore, this energy function has one extra freedom.

3.2.3 Regularization problem for $h = 2$ and $n = 2$ (2)

Another possible algorithm is the component-wise approach. First, we compute functions $F_1(\mathbf{x})$, $G_1(\mathbf{x})$, $F_2(\mathbf{x})$ and $G_2(\mathbf{x})$ by independently solving the following two standard regularization problems.

$$\begin{aligned} E^{(2,2a)}[F_1, G_1] &= \sum_{i=1}^{N} \left\{ \left(y_{1(i)}\right)^2 + G_1(\mathbf{x}_{(i)}) y_{1(i)} + F_1(\mathbf{x}_{(i)}) \right\}^2 \\ &\quad + \lambda_{F_1} \|S_{F_1} F_1(\mathbf{x})\|^2 + \lambda_{G_1} \|S_{G_1} G_1(\mathbf{x})\|^2, \end{aligned} \tag{31}$$

and

$$\begin{aligned} E^{(2,2b)}[F_2, G_2] &= \sum_{i=1}^{N} \left\{ \left(y_{2(i)}\right)^2 + G_2(\mathbf{x}_{(i)}) y_{2(i)} + F_2(\mathbf{x}_{(i)}) \right\}^2 \\ &\quad + \lambda_{F_2} \|S_{F_2} F_2(\mathbf{x})\|^2 + \lambda_{G_2} \|S_{G_2} G_2(\mathbf{x})\|^2. \end{aligned} \tag{32}$$

Then, by using the computed functions $\bar{G}_1(\mathbf{x})$ and $\bar{G}_2(\mathbf{x})$ of $G_1(\mathbf{x})$ and $G_2(\mathbf{x})$, we formulate the third standard regularization problem with respect to the function $H(\mathbf{x})$:

$$\begin{aligned} E^{(2,2c)}[H] &= \sum_{i=1}^{N} \left\{ 2y_{1(i)} y_{2(i)} + \bar{G}_2(\mathbf{x}_{(i)}) y_{1(i)} + \bar{G}_1(\mathbf{x}_{(i)}) y_{2(i)} + H(\mathbf{x}_{(i)}) \right\}^2 \\ &\quad + \lambda_H \|S_H H(\mathbf{x})\|^2 \end{aligned} \tag{33}$$

3.2.4 Inverse transformation of the transformation for linearization

The number of unknown functions has redundancy against the original functions. This redundancy makes it possible to choose a unique solution for the inverse transformation of transformation (29) as follows. First, we have two candidate solutions from functions $F_1(\mathbf{x})$, $F_2(\mathbf{x})$, $G_1(\mathbf{x})$, and $G_2(\mathbf{x})$,

$$\mathbf{f}_1(\mathbf{x}) = (f_{+,1}(\mathbf{x}), f_{+,2}(\mathbf{x}))^T, \quad \mathbf{f}_2(\mathbf{x}) = (f_{-,1}(\mathbf{x}), f_{-,2}(\mathbf{x}))^T, \tag{34}$$

and

$$\mathbf{f}_1(\mathbf{x}) = (f_{+,1}(\mathbf{x}), f_{-,2}(\mathbf{x}))^T, \quad \mathbf{f}_2(\mathbf{x}) = (f_{-,1}(\mathbf{x}), f_{+,2}(\mathbf{x}))^T, \tag{35}$$

where

$$f_{+,1}(\mathbf{x}) = \frac{1}{2} \left[-G_1(\mathbf{x}) + \sqrt{\{G_1(\mathbf{x})\}^2 - 4F_1(\mathbf{x})} \right], \tag{36}$$

$$f_{-,1}(\mathbf{x}) = \frac{1}{2}\left[-G_1(\mathbf{x}) - \sqrt{\{G_1(\mathbf{x})\}^2 - 4F_1(\mathbf{x})}\right], \tag{37}$$

$$f_{+,2}(\mathbf{x}) = \frac{1}{2}\left[-G_2(\mathbf{x}) + \sqrt{\{G_2(\mathbf{x})\}^2 - 4F_2(\mathbf{x})}\right], \tag{38}$$

and

$$f_{-,2}(\mathbf{x}) = \frac{1}{2}\left[-G_2(\mathbf{x}) - \sqrt{\{G_2(\mathbf{x})\}^2 - 4F_2(\mathbf{x})}\right]. \tag{39}$$

This two-fold ambiguity can be resolved by using the remaining function $H(\mathbf{x})$ by choosing a solution giving smaller a residual of

$$|H(\mathbf{x}) - f_{1,1}(\mathbf{x})f_{2,2}(\mathbf{x}) - f_{1,2}(\mathbf{x})f_{2,1}(\mathbf{x})| \tag{40}$$

at each point $\mathbf{x}$.

4 Conclusion

We have extended the standard regularization theory so that it can handle multi-valued functions. The representation of the multi-valued function is direct and no auxiliary field parameter is necessary. By simple substitutions of unknown functions, we have *standard* regularization problems, i.e., quadratic convex minimizations. This has a great advantage over conventional formalism including approaches using the line process and the multi-layer representations which have common difficulties in optimizations of their energy functionals.

The proposed extension has many possible scientific and engineering applications. Since the regularization theory provides a fundamental principle of the human early visual system, the proposed framework provides a model of multiple surface reconstruction for complex discontinuous surfaces and transparency perception.

The standard regularization theory also provides a general theory for spline approximations and (generalized) radial basis function ((G)RBF) methods for computational learning[21]. Our extensions can also help these methods to be extended into multi-valued functions. These subjects will be discussed elsewhere.

There are, however, several important remaining issues for future investigations as listed below.

1. The number of surfaces in entire space should be determined automatically. This can be viewed as a model selection problem. Theoretically, the degeneracy of the constraint satisfaction can indicate the redundant number of surfaces, and can be detected by computing the rank of the very large simultaneous linear system of the Euler-Lagrange equation (e.g. Eq. (12)). However, it is difficult to implement this test for such a large system. An alternative method is to evaluate the residual of the energy functional of each multiplicity and to use an information criterion to choose the most 'economical' model. This may be much easier to implement.

2. Local determination of the number of the surfaces is important for applications to discontinuous surface reconstruction problems. This may be possible with a local model selection algorithm or by testing the lack of supporting data.

3. The definition of distance is complicated, since the distance of a certain data point to multiple surfaces is not simple Euclidean distance to one of the surfaces. Accordingly, the noise model of the constraint equation is complicated due to the nonlinearity of the transformation between the transformed functions and the original functions. This makes the detection of intersection of surfaces an ambiguous and difficult problem. One solution to this problem is to impose the smoothness constraint on the original functions at the time of inverse transformations.

References

[1] Ando H (1993) A computational model for reconstructing multiple surfaces. Investigative Ophthalmology & Visual Science (Supplement) 34(4): 1186.

[2] Blake A, Zisserman A (1987) Visual Reconstruction. MIT Press Cambridge MA

[3] Darrel T, Sclaroff S, Pentland A (1990) Segmentation by minimal description. IEEE 3rd Int Conf Comput Vision, Osaka, Japan, pp.112-116

[4] Darrel T, Pentland AP (1991) Robust estimation of multi-layered motion representation. IEEE Workshop on Visual Motion, Princeton, pp.173-178

[5] Geiger D, Girosi F (1991) Parallel and deterministic algorithms from mrfs: surface reconstruction. IEEE Trans Patt Anal Machine Intell 13(5):401-412

[6] Geman S, Geman D (1984) Stochastic relaxation, Gibbs distributions and the Bayesian restoration of images. IEEE Trans Patt Anal Machine Intell 6:721-741

[7] Grimson WEL. (1981) From Images to Surfaces: A Computational Study of the Human Early Visual System. MIT Press Cambridge MA

[8] Harris JG, Koch C, Staats E, Luo J (1990) Analog hardware for detecting discontinuities in early vision. Int J Comput Vision 4: 211-223

[9] Horn BKP, Schunck BG (1981) Determining optical flow. Artif Intell 17:185-203

[10] Kersten D (1991) Transparency and the cooperative computation of scene attributes. In Computational Models of Visual Processing (Landy MS and Movshon JA eds) MIT Press Cambridge MA

[11] Kirkpatrick S, Gelatt CD, Vecchi MP (1983) Optimization by simulated annealing. Science 220: 219-227

[12] Madarasmi S, Kersten D, Pong T-C (1993) The computation of stereo disparity for transparent and for opaque surfaces. In Advances in Neural Info Proc Syst 5. Morgan Kaufman Publishers

[13] Marroquin JL (1992) Random measure fields and the integration of visual information. IEEE Trans Sys Man & Cybern 22: 705-716

[14] Noest AJ, Koenderink JJ (1990) Visual coherence despite transparency or partial occlusion. Perception 19: 384.

[15] Noest AJ (1993) Neural processing of overlapping shapes. Proc NATO Advanced Research Workshop 'Shape in Picture', Springer Verlag, Berlin.

[16] Penrose R (1989) The Emperor's New Mind: Concerning Computers, Minds, and the Laws of Physics. Oxford University Press, Oxford UK

[17] Poggio T, Torre V, Koch C (1985) Computational vision and regularization theory. Nature 317:314-319

[18] Poggio T, Koch C (1985) Ill-posed problems in early vision: from computational theory to analogue networks. Proc R Soc Lond B 226: 303-323

[19] Poggio T, Gamble E, Little JJ (1988) Parallel integration of vision modules. Science 242: 436-440

[20] Poggio T (1990) A theory of how the brain might work. Proc Cold Harbor Symp on Quantitative Biology IV: 899-910

[21] Poggio T, Girosi F (1990) Networks for approximation and learning. Proc IEEE 78(9): 1481-1497

[22] Prazdny K (1985) Detection of binocular disparities. Biol Cybern 52: 93-99

[23] Rosenfeld A, Jasinschi R(Eds.) (1993) Special Issue on Perceptual Transparency. Spatial Vision 7(2)

[24] Shizawa M (1993) Direct estimation of multiple disparities for transparent multiple surfaces in binocular stereo. Proc. IEEE 4th Int Conf Comput Vision (ICCV'93) Berlin Germany pp.447-454

[25] Shizawa M (1993) Extension of the standard regularization theory into multi-valued functions (1): reconstruction of smooth multiple surfaces via massively parallel relaxation (in Japanese). ATR Technical Report TR-H-027, September 1993

[26] Terzopoulos D (1986) Regularization of inverse visual problems involving discontinuities. IEEE Trans Pattern Anal Mach Intell 8: 413-424

[27] Tikhonov AN, Arsenin VY (1977) Solutions of ill-posed problems. W.H.Winston, Washington DC

[28] Wang JYA, Adelson EH (1993) Layered representation for motion analysis. IEEE Conf Comput Vision & Patt Recog, New York City, pp.361-366

[29] Weinshall D (1989) Perception of multiple transparent planes in stereo vision. Nature 341: 737-739

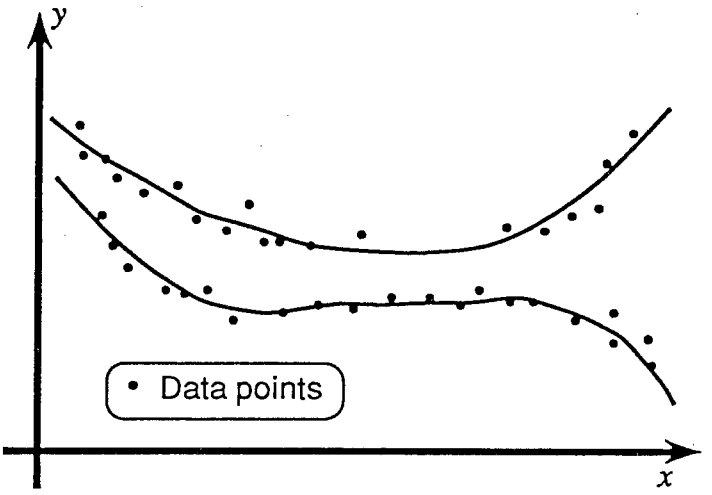

Figure 1: Example of data set that is characterized by two-fold surfaces (curves).

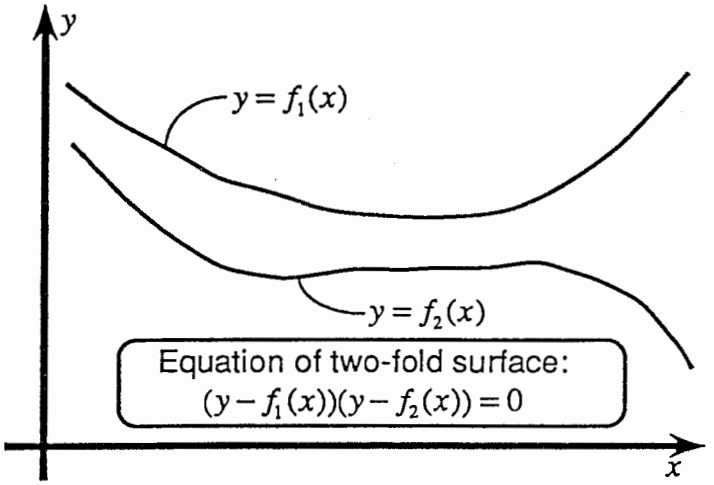

Figure 2: Constraint equation of two-fold surfaces.

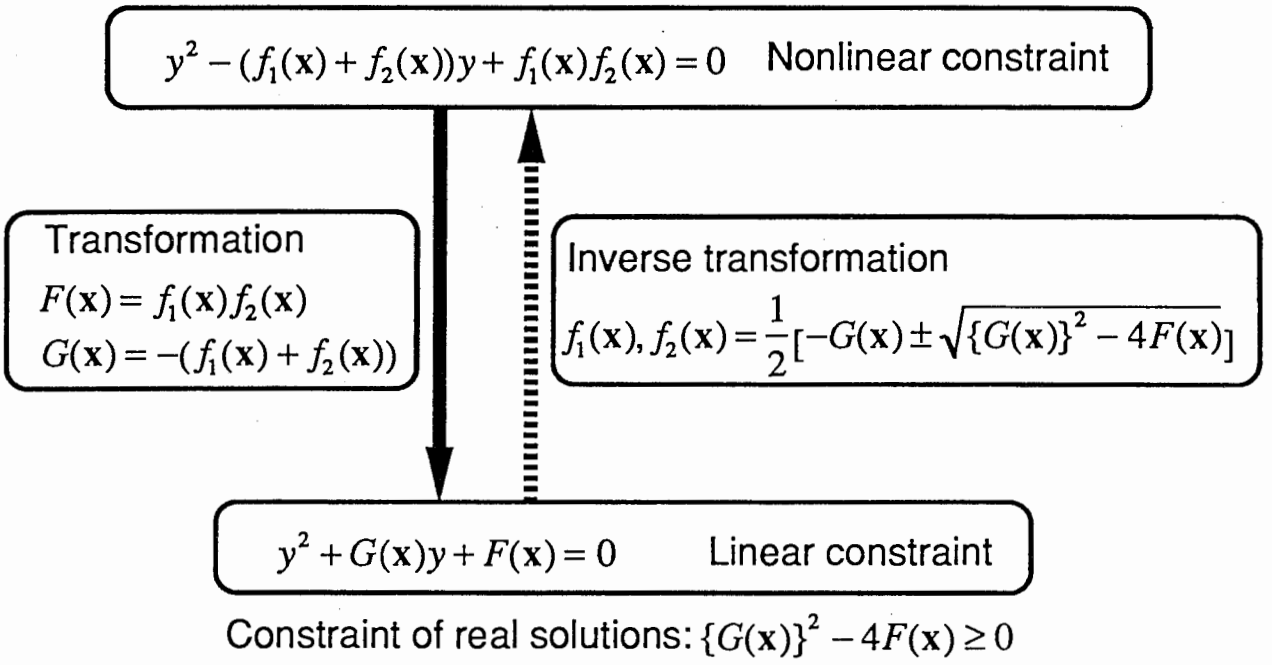

Figure 3: Transformation and inverse transformation for the linear constraint.

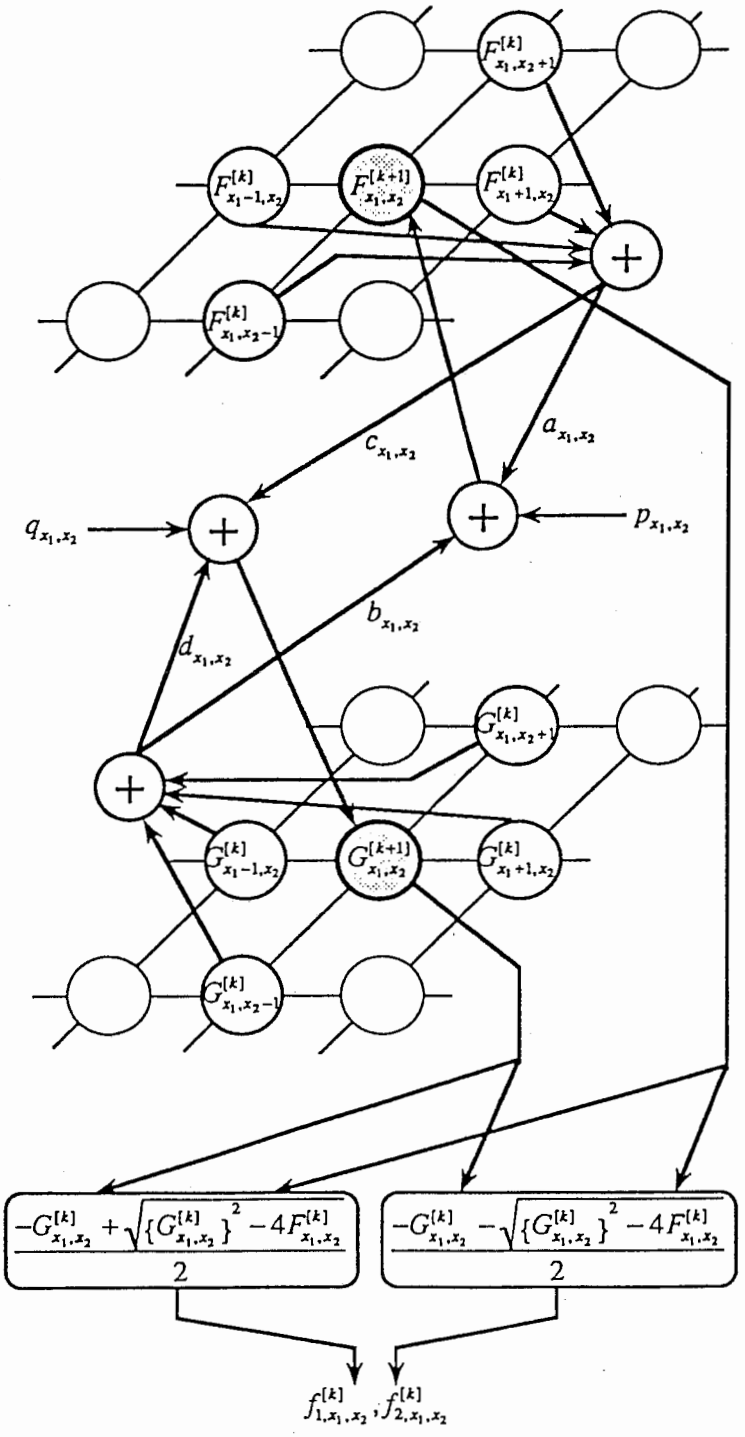

Figure 4: Network of Gauss-Seidel relaxation method for two-fold-surface reconstruction.

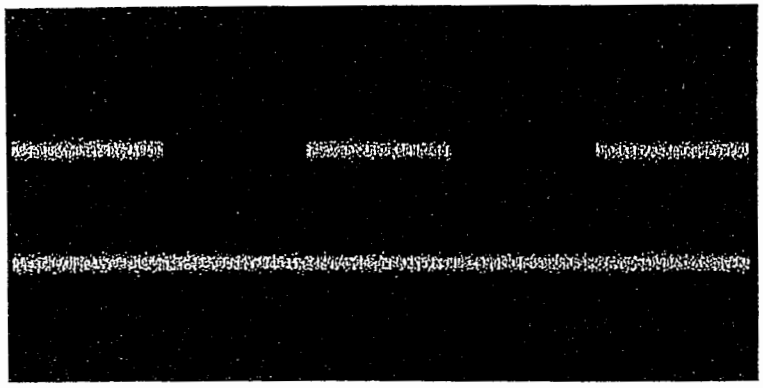

(a) Test Sample data (See text).

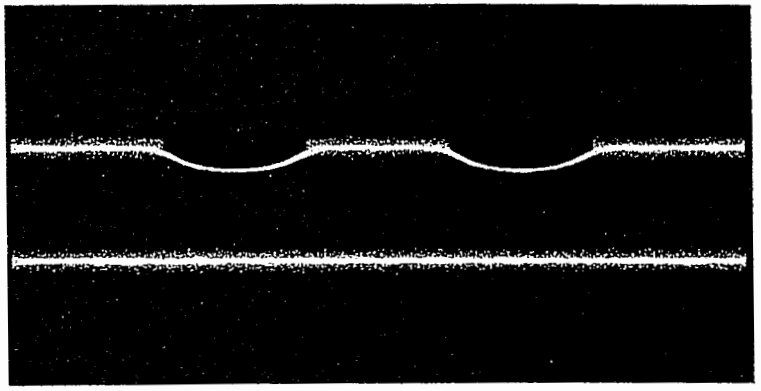

(b) Result after 500 iterations (side view).

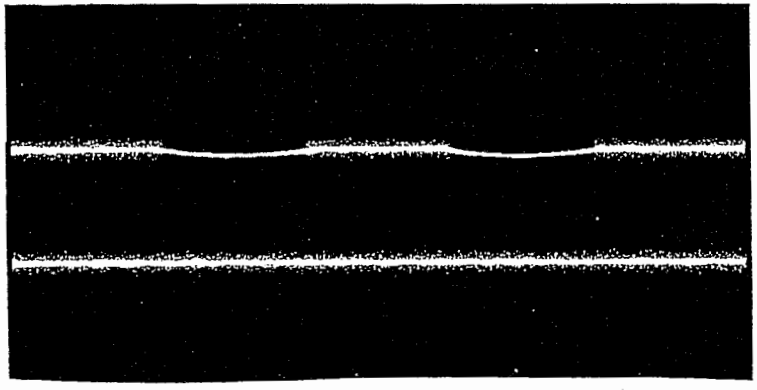

(c) Result after 10000 iterations (side view).

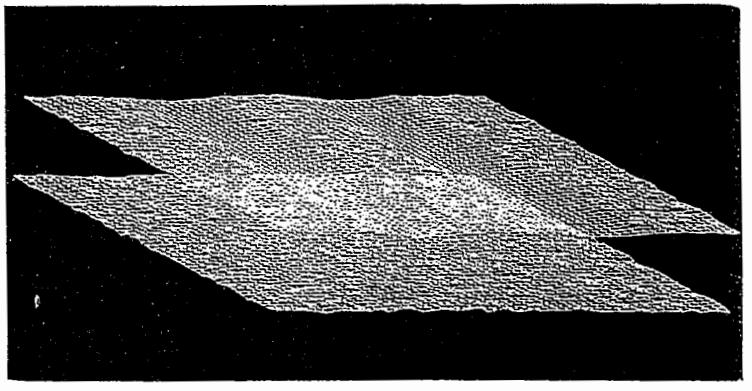

(d) Result after 10000 iterations.

Figure 5: Results of experiment #1.

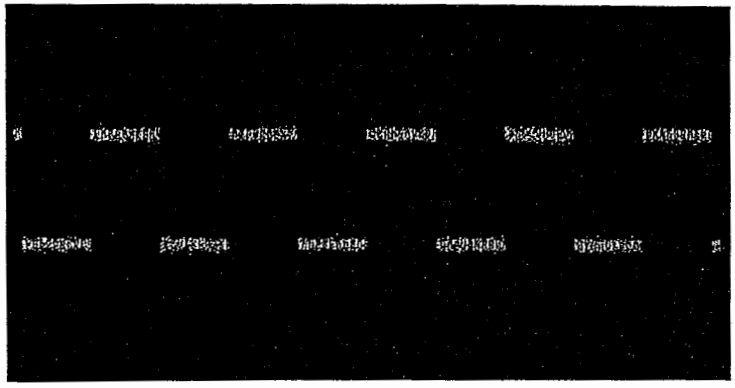

(a) Test Sample data.

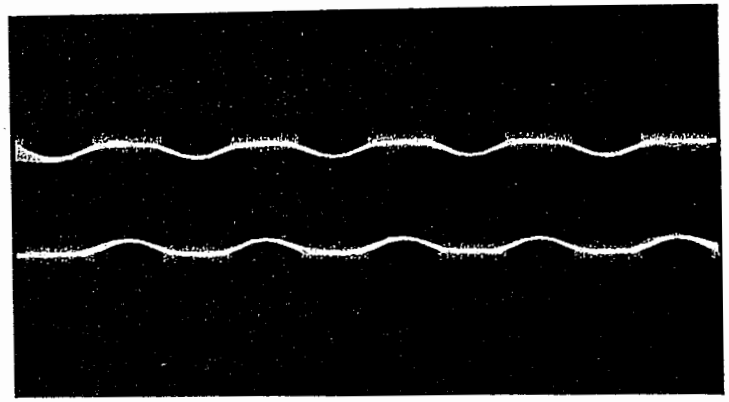

(b) Result after 500 iterations (side view).

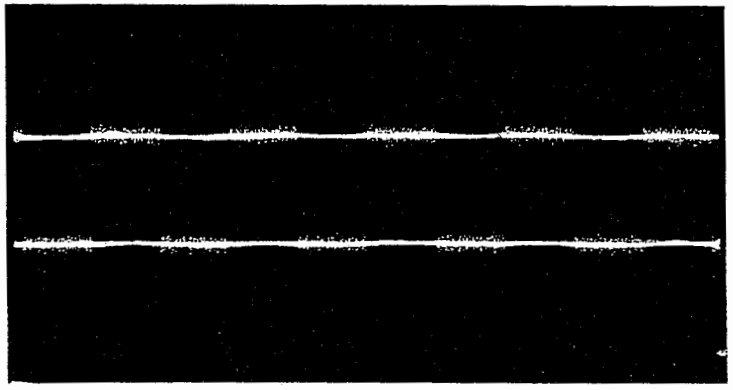

(c) Result after 10000 iterations (side view).

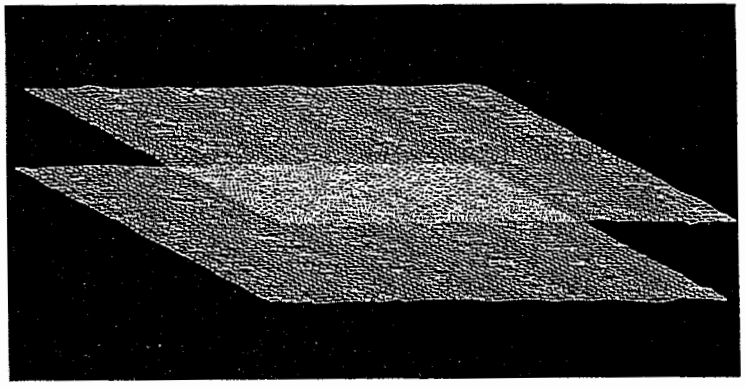

(d) Result after 10000 iterations.

Figure 6: Results of experiment #2.

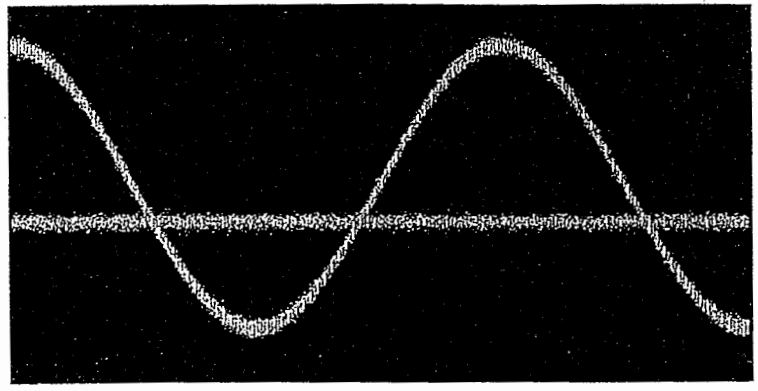

(a) Test Sample data (See text).

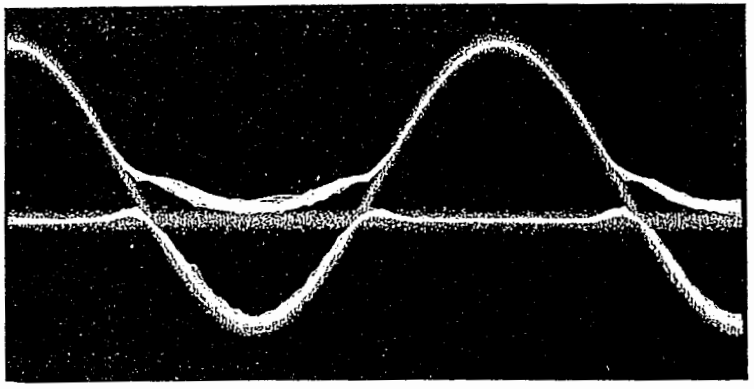

(b) Result after 500 iterations (side view).

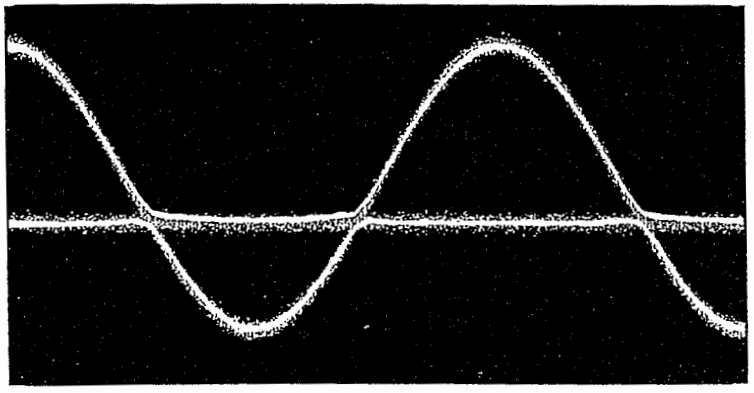

(c) Result after 2000 iterations (side view).

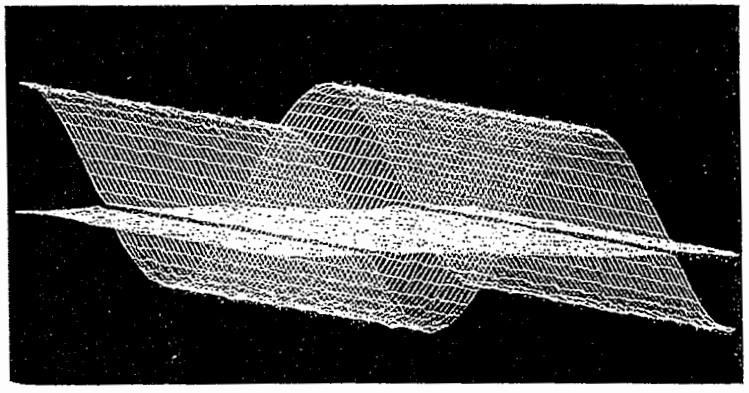

(d) Result after 2000 iterations.

Figure 7: Results of experiment #3.

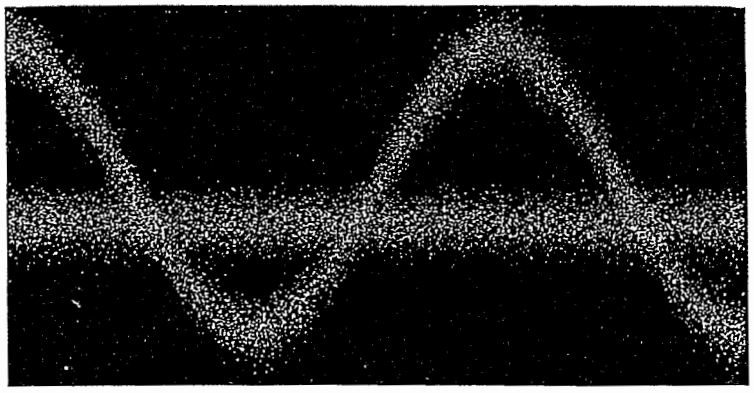

(a) Test Sample data (See text).

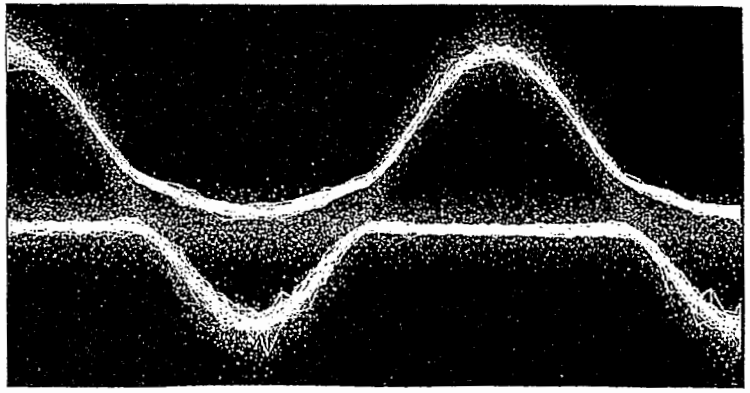

(b) Result after 500 iterations (side view).

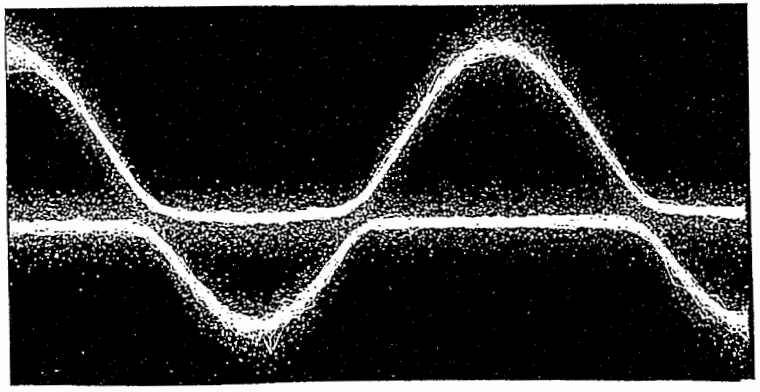

(c) Result after 2000 iterations (side view).

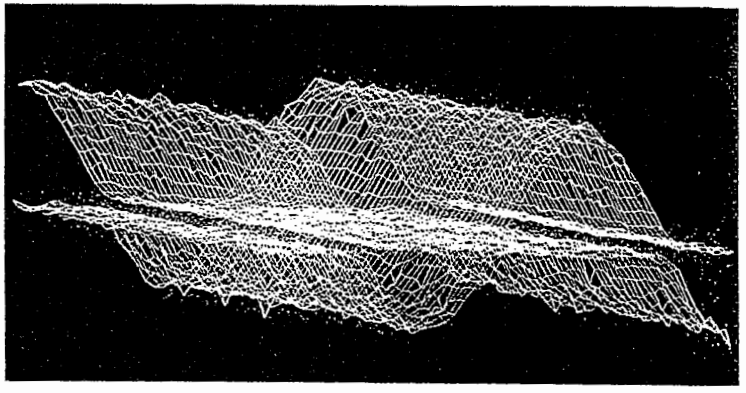

(d) Result after 2000 iterations.

Figure 8: Results of experiment #4.

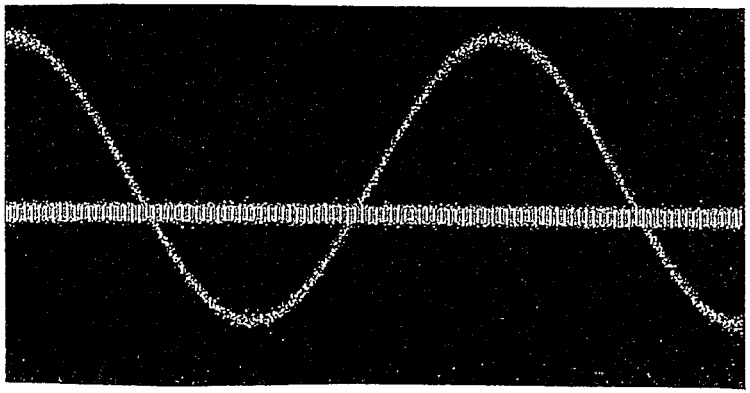

(a) Test Sample data (See text).

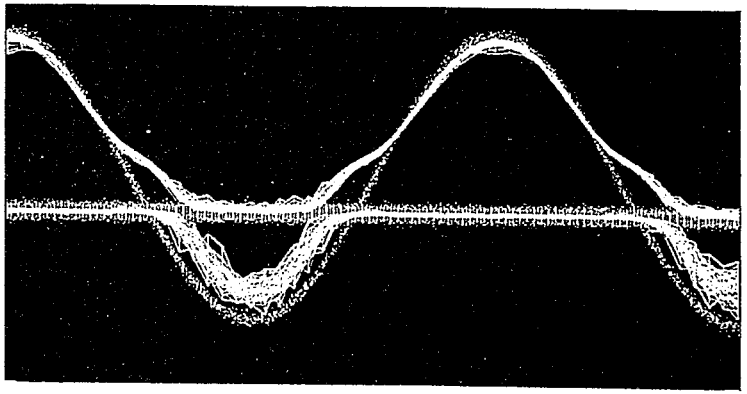

(b) Result after 500 iterations (side view).

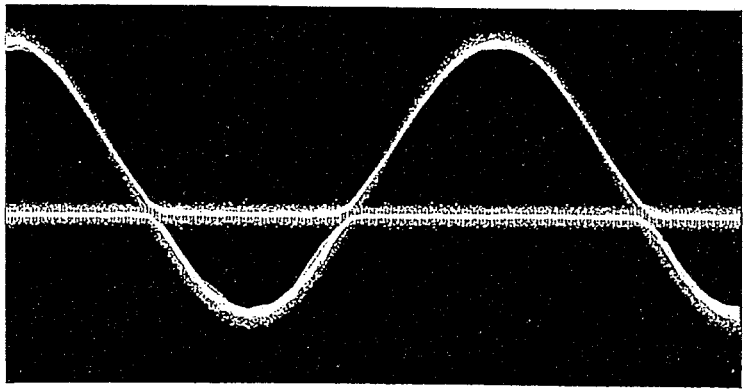

(c) Result after 2000 iterations (side view).

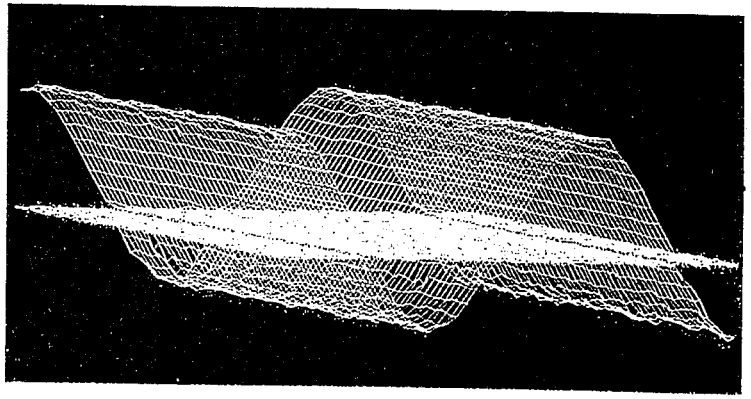

(d) Result after 2000 iterations.

Figure 9: Results of experiment #5.